

SEM Analysis of Ion Implanted SiC

Johan B Malherbe^{1*}, NG van der Berg¹, AJ Botha¹, E Friedland¹, TT Hlatshwayo¹,
RJ Kuhudzai¹, E Wendler², W Wesch², P Chakraborty³ & EF da Silveira⁴

¹D Department of Physics, University of Pretoria, Pretoria, 0002, South Africa

²Institut für Festkörperphysik, Friedrich-Schiller-Universität, 07743 Jena, Germany

³Saha Institute of Nuclear Physics, 1/AF Bidhannagar, Kolkata 700 064, India

⁴Physics Department, Pontificia Universidade Católica do Rio de Janeiro, Rio de Janeiro, Brazil

*Author for correspondence: johan.malherbe@up.ac.za

SiC is a material used in two future energy production technologies, firstly as a photovoltaic layer to harness the UV spectrum in high efficient power solar cells, and secondly as a diffusion barrier material for radioactive fission products in the fuel elements of the next generation of nuclear power plants. For both applications, there is an interest in the implantation of reactive and non-reactive ions into SiC and their effects on the properties of the SiC. In this study 360 keV Ag⁺, I⁺ and Xe⁺ ions were separately implanted into 6H-SiC and in polycrystalline SiC at various substrate temperatures. The implanted samples were also annealed in vacuum at temperatures ranging from 900°C to 1600°C for various times. In recent years, there had been significant advances in scanning electron microscopy (SEM) with the introduction of an in-lens detector combined with field emission electron guns. This allows defects in solids, such as radiation damage created by the implanted ions, to be detected with SEM. Cross-sectional SEM images of 6H-SiC wafers implanted with 360 keV Ag⁺ ions at room temperature and at 600°C and then vacuum annealed at different temperatures revealed the implanted layers and their thicknesses. A similar result is shown of 360 keV I⁺ ions implanted at 600°C into 6H-SiC and annealed at 1600°C. The 6H-SiC is not amorphized but remained crystalline when implanting at 600°C. There are differences in the microstructure of 6H-SiC implanted with silver at the two temperatures as well as with reactive iodine ions. Voids (bubbles) are created in the implanted layers into which the precipitation of silver and iodine can occur after annealing of the samples. The crystallinity of the substrate via implantation temperature caused differences in the distribution and size of the voids. Implantation of xenon ions in polycrystalline SiC at 350°C does not amorphize the substrate as is the case with room temperature heavy ion bombardment. Subsequent annealing of the implanted polycrystalline samples leads to increased thermal etching effects such as grain boundary grooving. Damage due to channelling (or non-channelling) in the different crystallites resulted also in differences in thermal etching in the crystallites.

Keywords: Nuclear materials, photovoltaic materials, SiC, SEM, implantation, microstructure, voids, bubbles, defects, topography

INTRODUCTION

Traditionally, scanning electron microscopy (SEM) has been used to characterize the topography of surfaces before and after ion bombardment [1, 2]. In recent years there had been significant advances in scanning electron microscopy (SEM) with the introduction of

an in-lens detector. This allows SEM images to be taken with very low voltages, resulting in more surface sensitive images to be obtained. Another advantage with an in-lens detector system in SEM is that some defects can become visible. Twins and/or stacking faults which are normally only detected with transmission electron microscopy (TEM) can easily be seen on SiC using in-lens SEM [3, 4].

Due to the Kyoto Protocol and global weather changes there is a demand to reduce the world's reliance on fossil fuel for power production. Consequently, many alternative power production technologies are being investigated. SiC is a material used in two future energy production technologies: As a photovoltaic layer to harness the UV spectrum in high efficient power solar cells, and as a diffusion barrier material for radioactive fission products in the fuel elements of the next generation of nuclear power plants.

For both applications, there is an interest in the implantation of reactive and non-reactive ions into SiC and their effects on the properties of the SiC. The semiconductor substrates of photovoltaic devices must be doped to create p-n junctions. In the case of SiC, the doping is usually done via ion implantation and annealing. In nuclear reactors energetic heavy ions are produced during the fission reaction. These ions can cause radiation damage in the SiC leading to radiation-enhanced and radiation-induced diffusion, thereby defeating the purpose of the SiC as being a diffusion barrier for the radioactive fission products [5, 6]. Furthermore, these ions can also chemically react with the SiC destroying its integrity and its diffusion barrier properties.

In this paper, several examples of modern SEM investigations of such ion bombarded SiC surfaces before and after vacuum annealing are given. These investigations explain some of the properties resulting from such treatments.

EXPERIMENTAL

Single crystal 6H-SiC (from *Intrinsic Semiconductors*[®]) and polycrystalline SiC (from *Valley Design Corporation*[®]) samples were investigated by field emission scanning electron microscopy (FEG-SEM) employing a *Zeiss Ultra 55* instrument fitted with the usual SEM detectors and an in-lens detector. This instrument can be operated at voltages as low as 500 eV. In this study, we mostly employed 2 kV in order to reduce the distorting effect on very low accelerating voltage SEM images of carbon build-up on the samples during electron beam exposure. With low accelerating voltages the sampling depth becomes smaller giving more representative picture of the morphology of the real surface. The in-lens detector gives SEM images which show defects present in the samples but at the expense of topographic detail which becomes more detectable with the normal SEM detector. In this paper only images taken in the in-lens mode are shown.

Some sample surfaces were prepared in the usual way TEM samples are prepared. The samples were glued together and cross-sectional samples were prepared by thinning and smoothing the samples by mechanical polishing. The final smoothing step for some of these samples were to bombard them with low energy Ar⁺ ions at glancing angles while rocking the samples nearly perpendicular to the interface.

360 keV Ag⁺, I⁺ or Xe⁺ ions were implanted at an incidence angle of 7° to fluences of 2 x 10¹⁶ cm⁻². A dose rate of about 1 x 10¹² cm⁻²s⁻¹ was used. Notwithstanding this relatively low rate,

temperature of the samples implanted at room temperature increased to about 50°C. To investigate the effect of substrate temperature during ion bombardment, some samples were implanted at 350°C and some at 600°C.

Some samples were vacuum annealed in a computer controlled *Webb* graphite furnace for different periods at temperatures ranging from 900 up to 1600°C. The base pressure prior to annealing was in the range 10^{-6} - 10^{-7} mbar. During annealing, the pressure sharply increased to a maximum of 5×10^{-5} mbar and then decreased to the 10^{-6} mbar range.

RESULTS AND DISCUSSION

Heavy ion bombardment of the covalent-bonded ceramic SiC at room temperature causes the substrate to become amorphous at relatively low doses [7]. However, it is generally accepted that implanting SiC at 350°C and at 600°C results in the SiC remaining crystalline albeit with many point defects present [7, 8].

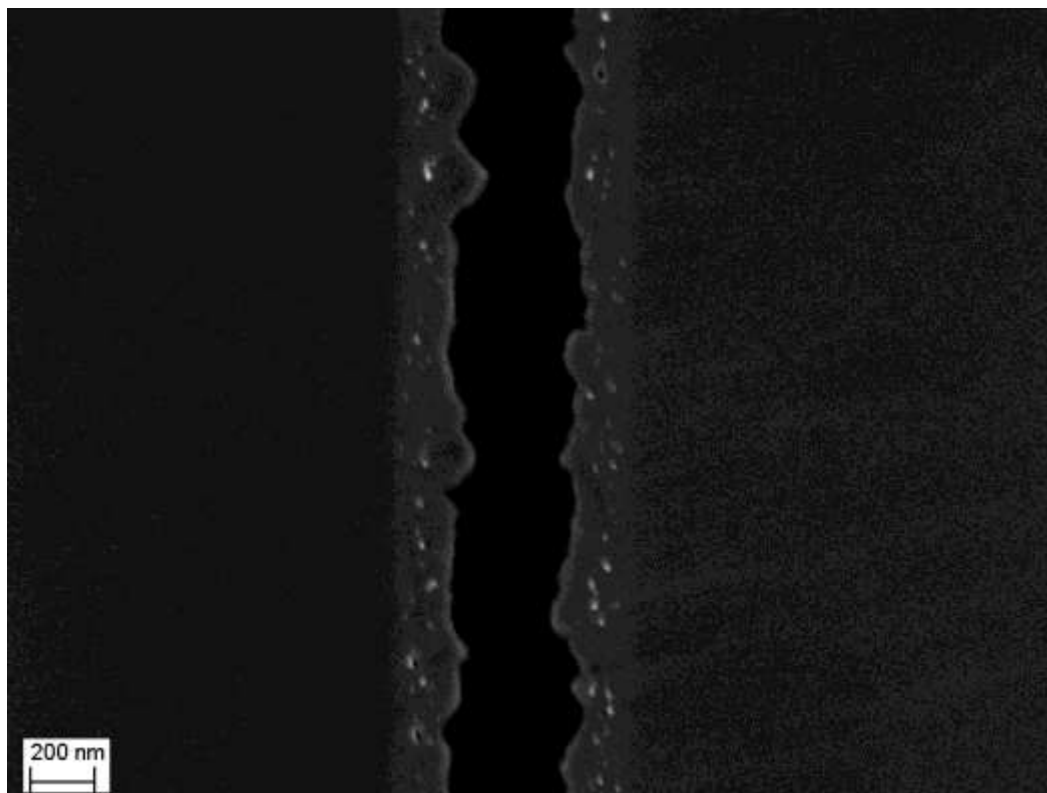


Figure 1. An in-lens SEM image of 6H-SiC bombarded by 360 keV Ag^+ ions at room temperature to a fluence of $2 \times 10^{16} \text{ cm}^{-2}$. The implanted sample was vacuum annealed at 900°C for 10h and again for 20 h at 1200°C. The sample was cut into two parts and glued together to form a sandwich. The image is a cross-section of the sandwiched sample. The middle black band is the glue that held the two samples together.

Figure 1 shows an in-lens SEM image of 6H-SiC bombarded by 360 keV Ag^+ ions at room temperature. After ion bombardment, the samples were first vacuum annealed for 10h at 900°C and then again for 20h at 1200°C. The reason for this double choice of

annealing conditions was to determine the effect of silver transport in a polycrystalline SiC substrate and not in amorphous SiC. Room temperature implantation of heavy ions (such as Ag) results in the complete amorphization of the implanted region of SiC. It is known [9, 10] that annealing at 900°C (which is below the melting point of silver) results in the recrystallization of the bombardment-induced a-SiC. Ag starts to diffuse in polycrystalline SiC only at about 1200°C [11, 12]. Three features in Figure 1 are of interest for this paper. There is a whitish band approximately 150 nm wide from the surface. The projected range of 360 keV Ag⁺ ions in 6H-SiC with density of 3.215 g/cm³ [13] is 110 nm and the projected range straggling 27 nm [14]. Consequently, the width of the white band corresponds to the width of the implanted layer in the SiC. The uniformity of the colour across the layer is an indication that the white band represents the damaged layer. This layer was originally the bombardment-induced amorphized layer which was recrystallized by the annealing steps as discussed above. However, our channelling studies [15 - 17] show that the layer still contains damage after annealing – also visible in Figure 1 as the white band. This is in agreement with other observations of defect detection in SiC with an in-lens SEM [3, 4]. Another feature in Figure 1 is the small bright spheres in the implanted layers. From a comparison of the SEM and backscattering images, it followed that these spheres were silver precipitates resulting from the diffusion and conglomeration of the implanted silver atoms during the annealing process. This conglomeration of implanted species in 6H-SiC into nanocrystals after annealing above 1200°C has been previously observed for other elemental implants - see [9] for a review. These nanocrystals were only observed after high temperature implantation (typically 700°C to retain crystallinity of the substrate) and subsequent annealing at 1600°C. The majority of these precipitates in Figure 1 are also in the region of the projected range of the implanted silver which confirms our premise that they are Ag nanocrystals. EBSD (Electron Back Scattered Diffraction) measurements performed on crystallites showed them to be 3C-SiC. Due to the low solubility of Ag in SiC, the silver atoms segregate out of SiC crystallites. The precipitates are probably tetrahedrally bounded by {111} planes. The reason being that the {111} plane has the lowest surface energy [9]. The final feature of Figure 1 is the unevenness of the implanted surfaces. After implantation, the implanted surfaces were completely featureless because of the amorphization of the 6H-SiC by silver ion bombardment at room temperature [15, 16]. Vacuum annealing at temperatures above 800°C caused recrystallization of the amorphous SiC – see Figure 2. RBS/channelling investigations showed that there is gradual (depending on the annealing temperature) epitaxial regrowth taking place from the amorphous-crystalline interface [16]. In Figure 2, numerous small crystallites are visible with random orientation indicating that the crystalline substrate played no role in the recrystallization process.

Our RBS/channelling studies [17] showed that in contrast to room temperature implantation, silver ion bombardment at 600°C resulted in the 6H-SiC remaining single crystalline albeit with point defects due to the presence of the implanted foreign silver atoms. RBS measurements [16, 17] indicated that there is also no transport / diffusion of the implanted Ag in single crystalline SiC even at higher annealing temperatures (i.e. 1500°C) in contrast to that in polycrystalline SiC as shown in Figures 1 and 2. In Figure

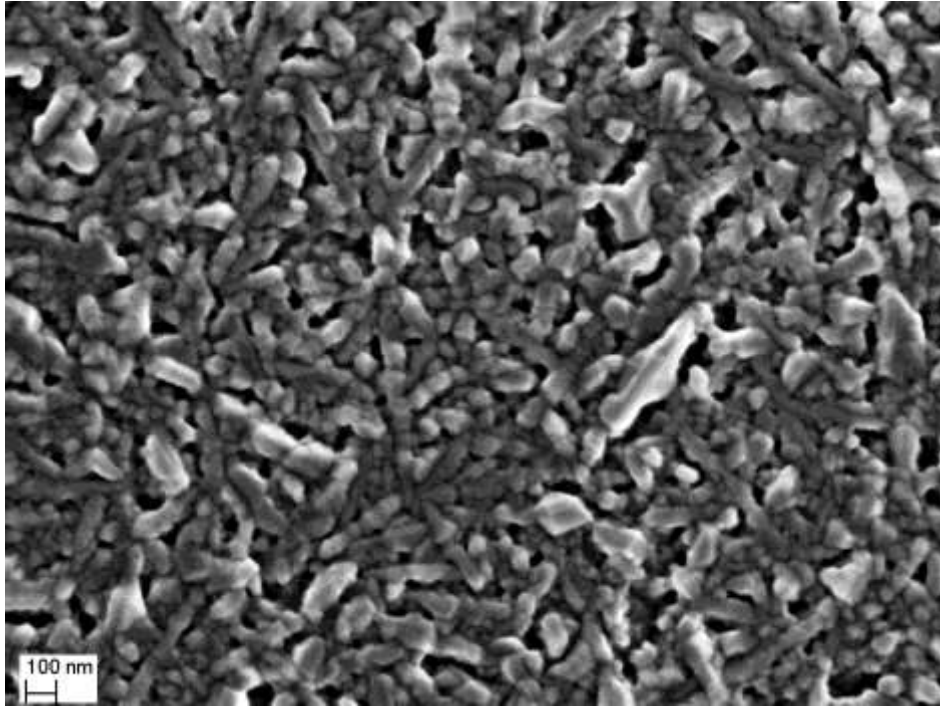


Figure 2. An in-lens SEM image of a 6H-SiC surface bombarded by 360 keV Ag^+ ions at room temperature and then vacuum annealed at 900°C for 10h and again for 20 h at 1200°C. The image show that the annealed surface consists of crystallites with random orientation.

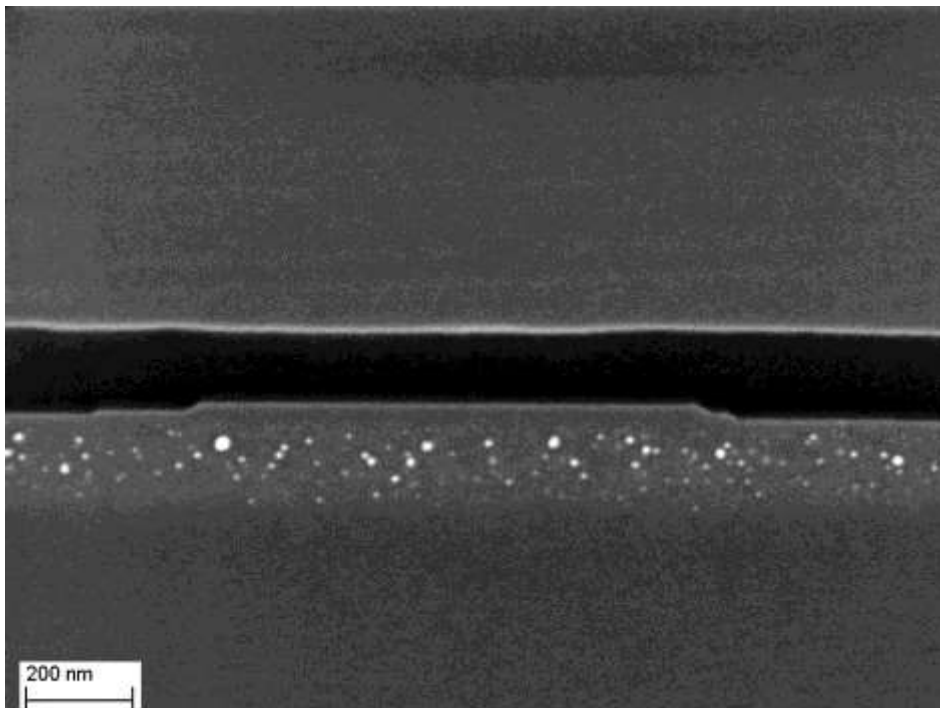


Figure 3. An in-lens SEM image of a cross-section surface of a sandwiched sample of 6H-SiC bombarded by 360 keV Ag^+ ions at 600°C to a fluence of $2 \times 10^{16} \text{ cm}^{-2}$ and virgin 6H-SiC substrate (at the top). The implanted sample was vacuum annealed at 1500°C for 6 h. After annealing the samples were glued together to form a sandwich. The middle black band is the glue that held the two samples together.

3, a cross-sectional SEM image of a 600°C Ag implanted 6H-SiC sample annealed at 1500°C for 6h shows again small silver precipitates in the 6H-SiC which precipitated during the annealing process. However, in contrast to the room temperature implanted case, these precipitates are more evenly spaced throughout the whitish implanted band indicating that the crystalline structure did not allow the formation of large openings in the SiC for the conglomeration/precipitation of Ag into relatively large (as was the case for the room temperature implanted samples which were amorphous after the ion bombardment) silver precipitates. These smaller and more evenly spread Ag precipitates in the single crystalline 6H-SiC compared to the larger Ag precipitates in the polycrystalline SiC layer shown in Figures 1 and 2 can be understood from the mechanisms of their formations. TEM investigations [18] of Ge and Er high temperature implanted nanocrystals showed that the Ge and Er atoms segregated to dislocation cores to form the nanoprecipitates. One can expect the same mechanism for the silver precipitates. Again the implanted 6H-SiC surface (see Figure 3) does not appear completely flat. After the 600°C implantation process, SEM images of the implanted surfaces were featureless as is expected of a flat single crystal surface. The uneven surface in Figure 3 is due to step bunching occurring during the high temperature (1500°C) vacuum annealing [3, 19]. Step bunching is the conglomeration of steps and the formation of multiple-height steps on crystal surfaces. Step bunching also occurs during epitaxial growth which is a step-flow mechanism [20]. Since crystal growth and thermal etching are essentially similar

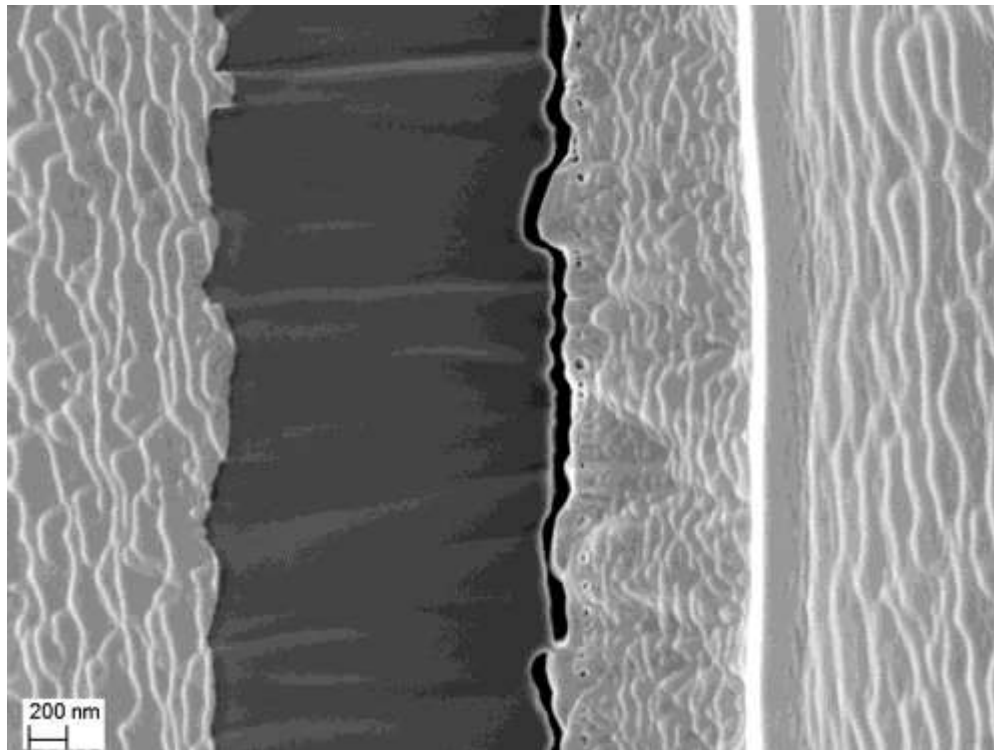


Figure 4. An in-lens SEM image of a cross-section surface of a sandwiched sample of 6H-SiC bombarded by 360 keV I^+ ions at room temperature to a fluence of $2 \times 10^{16} \text{ cm}^{-2}$ and a virgin 6H-SiC substrate (on the left). The implanted sample was vacuum annealed at 1600°C for 5 h. After annealing the samples were glued together to form a sandwich. The middle black band is the glue that held the two samples together. During the mechanical polishing process the bond broke between the glue and the implanted sample surface.

processes at the two extreme regimes, step bunching is used as evidence of thermal etching on single crystal surfaces [3, 19]. Thermal etching is the preferential sublimation of some crystal surfaces due to differences in the surface binding energies of the different surfaces. The formation of SiC “islands” due to step bunching as depicted in Figures 3 will have a detrimental effect on RBS depth profiling. The silver RBS profile will broaden making it appear as if the silver is diffusing more than it might in reality.

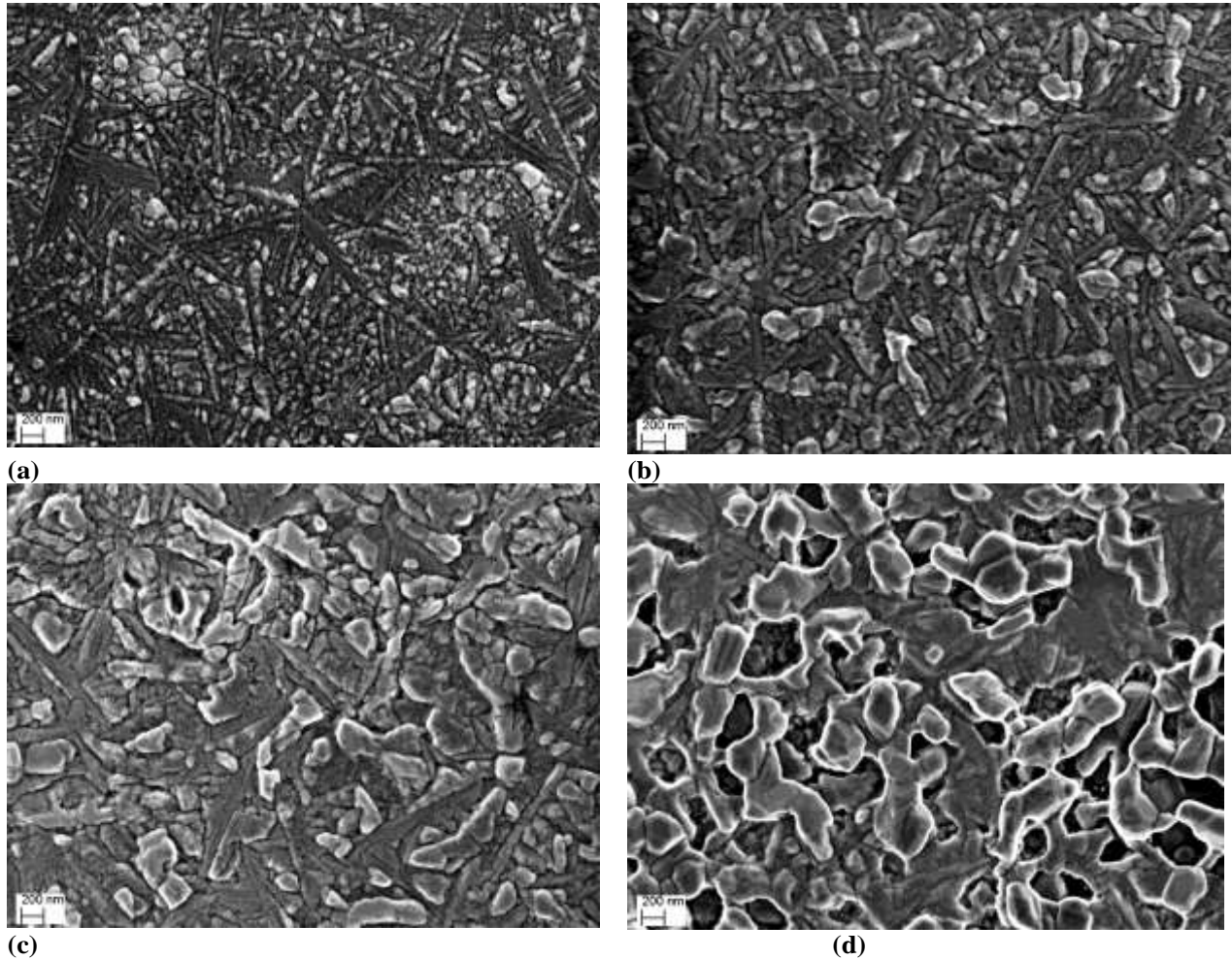


Figure 5. In-lens SEM images of room temperature iodine implanted 6H-SiC surfaces after vacuum annealing at 1100°C for (a) 5 h, (b) 60 h, and after vacuum annealing at 1200°C for (c) 5 h, and (d) 60 h.

Implanting 6H-SiC with reactive ions such as iodine leads to differences in the microstructure of the 6H-SiC compared to the inert Ag implantation. Figure 4 shows an in-lens SEM image of a cross-section of room temperature I^+ implanted 6H-SiC sample vacuum annealed afterwards at 1600°C for 5 h. The higher annealing temperature for the iodine implanted samples compared to the silver samples was chosen to compare our results to other reported nanoprecipitates in 6H-SiC as summarised in reference [9]. Holes are visible at about the projected range of the 360 keV iodine ions in SiC. The origin of these holes is similar to the Ag precipitates seen in Figures 1 and 3. In the SEM image in Figure 5, the holes are dark indicating that there is no or little iodine left in these openings. The reason for the absence of iodine in these voids, is related to the

thermal and sputter properties of iodine. Iodine is an element which volatilizes at room temperature due to its low heat of vaporization of 41.57 kJ/mol. During the final surface smoothing process of low energy Ar⁺ ion bombardment, the temperature of the substrate increased substantially above room temperature allowing the elemental iodine in the openings to sublime. Furthermore, iodine sputters more easily than SiC. Therefore, it will also be preferentially eroded from the holes.

Another difference with the silver implanted samples is the enhanced topography development on the 6H-SiC surface. In Figure 5, SEM images of room temperature I⁺ implanted 6H-SiC samples vacuum annealed at 1100°C and at 1200°C for two different annealing times of 5 h and 60 h, show the development of the surface topography from the flat featureless surface of an as-implanted surface. For the 1100°C 5h annealed sample, the surface consists of many dendritic crystals stretching radially out from a point – see Figure 5(a). There appears to be sections composed of closely packed small crystals and regions in between the crystallites where the surface seems flat and featureless – probably amorphous regions. The crystallization on the surface appears to be independent of the underlying crystalline region as the crystals grew randomly with no preferred orientation. This indicates that the crystal growth was not epitaxially from the crystalline substrate but originated from small recrystallized seed crystals within the bombardment-induced amorphized layer. Some of the crystallites are protruding more than others in line with the flow-step model of crystal growth of Burton et al. [20] and Hirsch and Pound [21]. As expected from this model, some surface crystals grew parasitically larger with annealing time. After annealing for 60 hours (see Figure 5(b)), the featureless regions had disappeared. The sample surfaces remained fairly continuous at this temperature with no clear indications of cavities or holes forming on the surface. At 1200°C, the crystallites were larger than to those formed at 1100°C. At this temperature, cavities appeared. Even for the 5 h annealed samples (see Figure 5(c)), the surface appears to be less continuous and cavities could be seen on the surface. The samples annealed for 5h still had dendritic crystal starting from a point. For longer annealing times, the sizes of the crystals became larger, overlapping with each other, causing the “growth” points to become less noticeable. The number and size of the cavities increased with annealing time. The crystallites are faceted. After annealing for 60 h many large cavities were formed – see Figure 5(d). These trends in increasing annealing temperatures and increasing annealing times continued to eventually result in the severe surface topography evident in Figure 4. This severe topography development follows from a step-flow epitaxial process where some crystal surfaces, i.e. the ones with the high surface energies, grow preferentially to expose more low energy surface areas in agreement with Wulff’s Law [22].

The logical explanation for the difference in the microstructure between silver and iodine implanted 6H-SiC is the difference in the chemistry of the implanting species with the substrate. No known compound is formed between Ag and Si, C or SiC. It is known [23, 24] that iodine reacts with Si to form SiI₄ which reacts further with silicon at higher temperatures to form SiI₂. However, SiI₂ is also known to be unstable at high temperatures (above 1000°C). No other compound between iodine and C or SiC has been reported. The difference in the microstructure suggests that there might be a possibility of such compounds forming, whether stable or unstable. EDX (Energy-Dispersive X-ray spectroscopy) done on our iodine implanted samples did not detect any iodine. This is not surprising as the excitation/analysis volume and depth of EDX are

orders of magnitude larger than the implanted layer depth and volume.

Furthermore, there have been reports that iodine aids in the growth 3C-SiC. Ramesh et al. [25] reported that pure 3C-SiC is obtained when heating Si and activated carbon powder in an iodine atmosphere in a commercial microwave oven. This is reminiscent of another 3C-SiC growth process using another halogen element Cl. During the growth of stoichiometric polycrystalline 3C CVD SiC using a Cl containing precursor methyltrichlorosilane (CH_3SiCl_3) a hydrogen mixture HCl is formed. Papisoulitis et al [26] found that the presence of HCl has several benefits for CVD SiC, inter alia the uniformity of the SiC and a complete suppression of free Si. The model of I conductivity to grow stoichiometric SiC is doubted by Pedersen et al [27]. Pedersen quoted that the average bond enthalpies at 25 °C for the Si-Si, Si-Cl, and Si-I bonds are 226, 400, 234 kJ mol^{-1} , respectively. According to Pedersen, the best choice is chlorine since the iodine atom is too large and a too weak bond to Si.

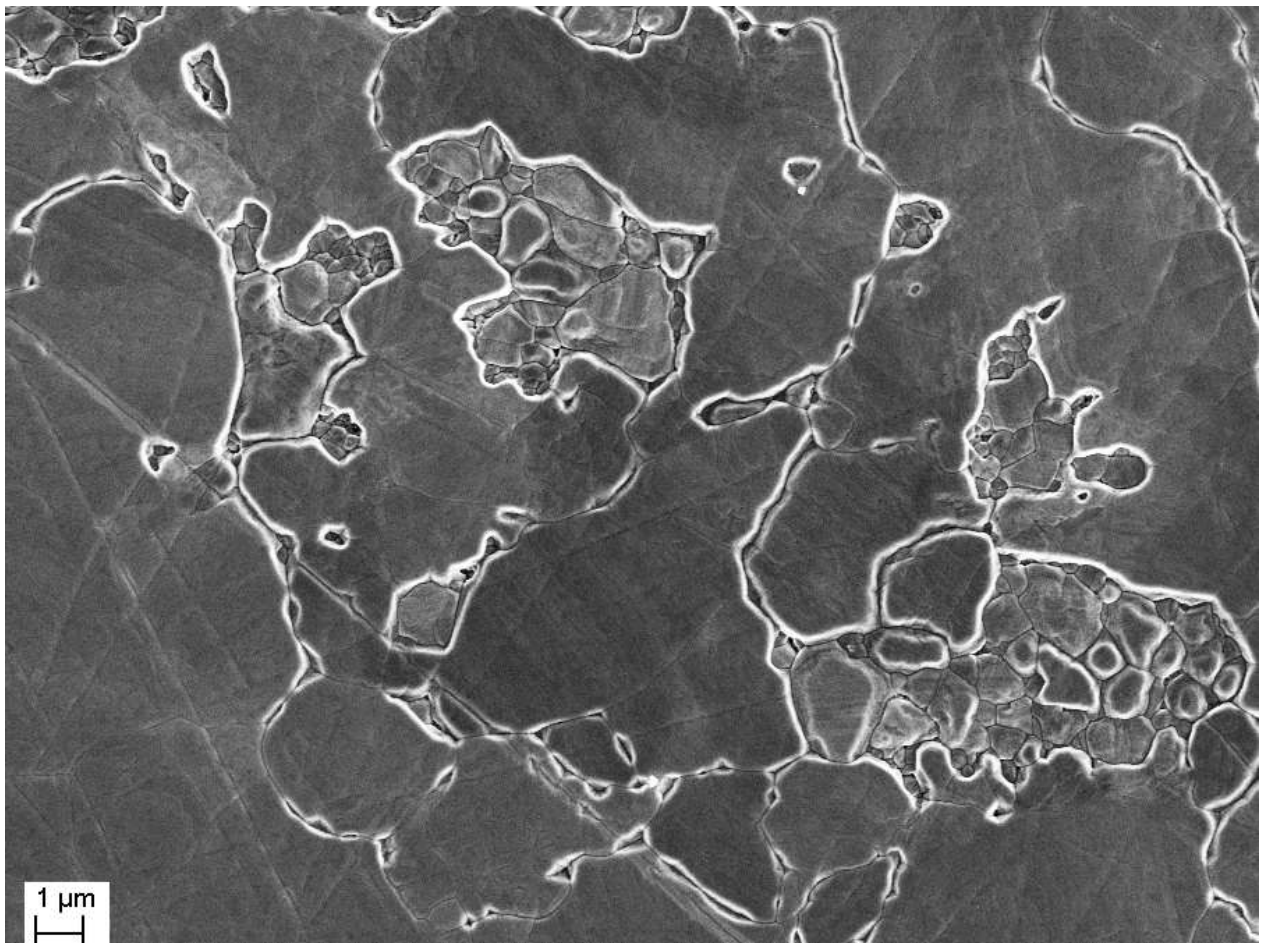


Figure 6. An in-lens SEM image of 350°C Xe^+ implanted polycrystalline SiC and then vacuum annealed at at 1200°C for a total of 40 h consisting of 4 annealing stages of 5 h + 5 h + 10 h +20 h.

Heavy ion implantation of polycrystalline SiC at room temperature amorphizes the substrate similarly as in the case of 6H-SiC, to render a flat featureless surface. However, implanting at even 350°C causes the implanted region to remain polycrystalline. When vacuum annealing these samples, changes appear between implanted and unimplanted SiC similarly treated. In

Figure 6, a polycrystalline SiC substrate is shown which was implanted with 360 keV Xe⁺ ions and subsequently vacuum annealed at 1200°C for a total of 40 h consisting of 4 annealing stages of 5 h + 5 h + 10 h +20 h. In Figure 7, an unimplanted part of the same (implanted) polycrystalline SiC sample is shown. On both SEM images, scratch marks from the factory polishing process are visible as well as the grains boundaries of the crystallites. Many of the grain boundaries of the implanted sample are pronouncedly etched (i.e. grain boundary grooving) because of thermal etching occurring during the vacuum annealing. This opening up of high angle boundaries by thermal etching is due to increased stress/strain caused by the large implanted atoms in interstitial positions. The surface regions of some of the grains were severely etched. In contrast, limited thermal etching occurred at the grain boundaries of the unimplanted sample. The surface regions of the grains were also not etched to the same extent as in the implanted sample. The differences are due to the radiation damage in the SiC introduced by the bombarding xenon ions. The extent of the radiation damage in each crystallite depends on the orientation of the crystallite, i.e. the damage will be deeper in crystallites with on-axis orientation allowing channelling to take place. This effect coupled with difference between the surface energies of different crystal orientations caused increased thermal etching to occur in those regions with high surface energies in order to expose lower surface energy areas thereby lowering the total energy of the system in agreement with Wulff's Law [22].

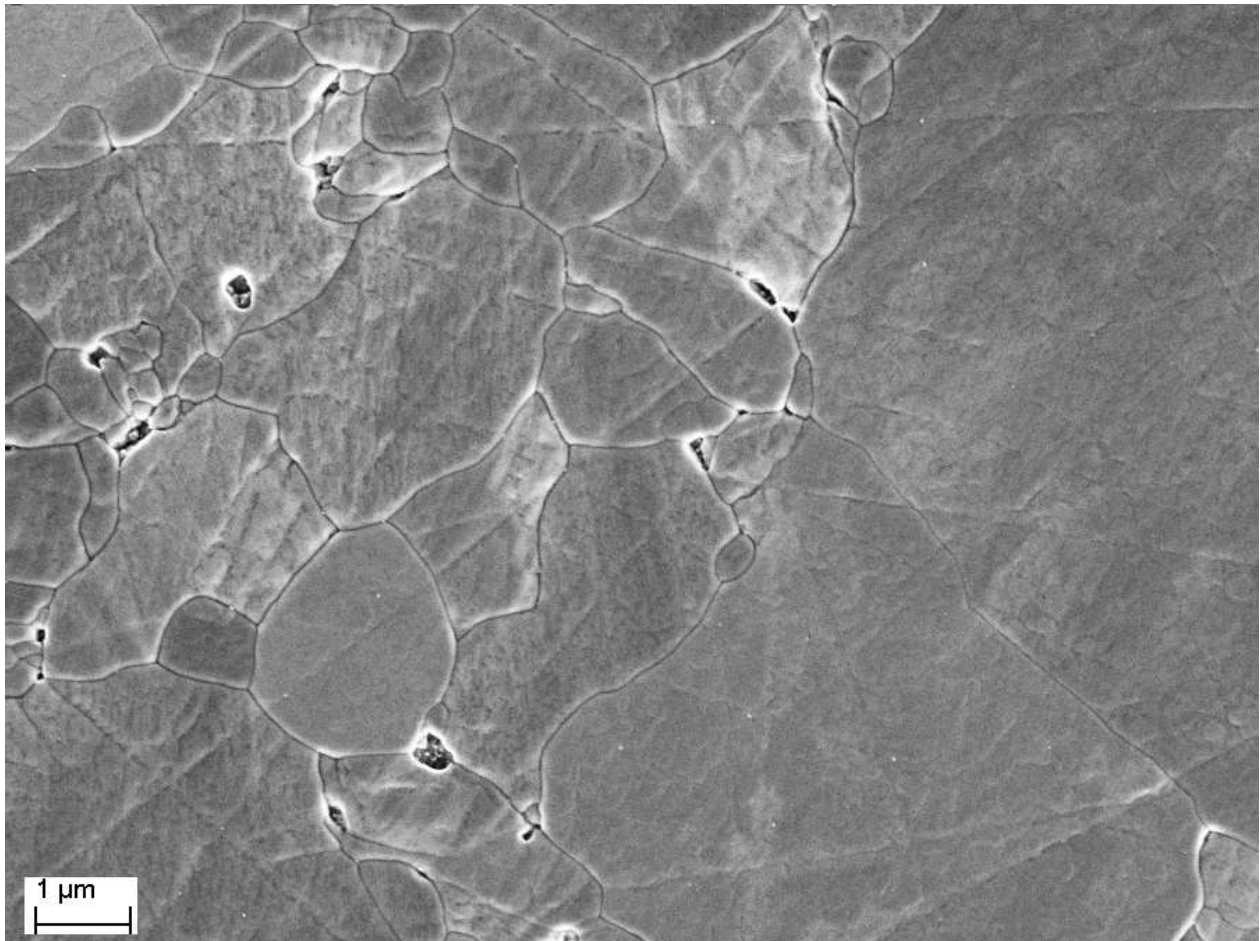


Figure 7. An in-lens SEM image of an unimplanted part of the sample shown in Figure 6.

SUMMARY

Modern high resolution SEMs with in-lens detector systems are capable of detecting crystal defects which are traditionally only possible to detect using TEM with its demanding sample preparation steps. This paper shows how this property can be used to observe the implanted layer and its thickness with SEM with considerably less effort in sample preparation than with TEM.

Annealing of Ag implanted SiC showed that the metastable solid solute of implanted Ag atoms in SiC is transformed into SiC with Ag precipitates. There are differences in the Ag conglomeration between room temperature and elevated temperature implanted 6H-SiC. The voids (bubbles) in the elevated temperature implanted layer are generally smaller and are spread throughout the implanted layer. This is due to the difference in the implant precipitation mechanisms between the two substrates. In the case of the elevated temperature implanted SiC with its retained crystallinity, the implanted material precipitates at dislocation cores. In polycrystalline SiC, the precipitation occurs between grains bordering with low energy surfaces.

The microstructure of 6H-SiC implanted with the iodine ions and then annealed are different to Ag implanted 6H-SiC. Step bunching became evident in the 1600°C annealed samples due to the occurrence of thermal etching. At lower annealing temperatures, dendritic crystallites grow from growth points radially out until they start overlapping with one another. The crystallites are larger than in the case of Ag implantation with large openings; some even reaching the unimplanted bulk indicating a step-flow epitaxial process where some crystal surfaces, i.e. the ones with the high surface energies, grow preferentially to expose more low energy surface areas.

Implanting and annealing polycrystalline SiC with Xe ions at elevated (350°C) temperatures allows the SiC to remain polycrystalline. Annealing at 1200°C caused grain boundary grooving to occur at the high angle boundaries. This grain boundary grooving was due to increased stress/strain caused by the large implanted atoms in interstitial positions. Damage due to channelling (or non-channelling) in the different crystallites resulted also in differences in thermal etching in the crystallites.

REFERENCES

1. J.B. Malherbe, *Critical Rev. Solid State Mater. Sci.* 19 (1994) 129.
2. O. Auciello and R. Kelly, *Ion Bombardment Modification of Surfaces*, Elsevier, Amsterdam 1984.
3. N.G. van der Berg, J.B. Malherbe, A.J. Botha and E. Friedland, *Appl. Surf. Sci.* 258 (2012) 5561.
4. N.G. van der Berg, J.B. Malherbe, A.J. Botha, E. Friedland and W.A. Jesser, *Surf. Interface Anal.* 42 (2009) 1156 -1159; *ibid* 1377.
5. J.B. Malherbe, E. Friedland, N.G. van der Berg, *Nucl. Instr. Methods Phys. Res. B*266 (2008) 1373.

6. E. Friedland, N.G. van der Berg, J.B. Malherbe, E. Wendler & W. Wesch, *J. Nucl. Mater.* 425 (2012) 205.
7. W. Wesch, A. Heft, E. Wendler, T. Bachmann, E. Glaser, *Nucl. Instrum. Methods Phys. Res. B* 96 (1995) 335.
8. E. Wendler, A. Heft, W. Wesch *Nucl. Instrum. Methods Phys. Res. B* 141 (1998) 105.
9. J.B. Malherbe, *J. Phys. D Appl. Phys.* (2013) To be published.
10. L.L. Snead and S.J. Zinkle, *Nucl. Instrum. Meth. Phys. Res. B* 191 (2002) 497.
11. E.K.H. Friedland, J.B. Malherbe, N.G. van der Berg, T. Hlatshwayo, A.J. Botha, E. Wendler & W. Wesch, *J. Nucl. Mater.* 389 (2009) 326.
12. E. Friedland, N.G. van der Berg, J.B. Malherbe, J.J. Hancke, J.R.N. Barry, E. Wendler & W. Wesch, *J. Nucl. Mater.* 410 (2011) 24.
13. L.L. Snead, T. Nozawa, Y. Katoh, T.-S. Byun, S. Kondo and D.A. Petti, *J. Nucl. Mater.* 371 (2007) 329.
14. J.F. Ziegler, M.D. Ziegler and J.P. Biersack, SRIM-2006, <http://srim.org/>, 5 Nov. 2006..
15. E.K.H. Friedland, J.B. Malherbe, N.G. van der Berg, T. Hlatshwayo, A.J. Botha, E. Wendler & W. Wesch, *J. Nucl. Mater.* 389 (2009) 326.
16. T.T. Hlatshwayo, J.B. Malherbe, N.G. van der Berg, L.C. Prinsloo, A.J. Botha, E. Wendler and W. Wesch, *Nucl. Instrum. Methods Phys. Res. B* 274 (2012) 120.
17. T.T. Hlatshwayo, J.B. Malherbe, N.G. van der Berg, A.J. Botha and P. Chakraborty, *Nucl. Instrum. Methods Phys. Res. B* 273 (2012) 61.
18. U. Kaiser, D.A. Muller, J.L. Grazul, A. Chuvilin and M. Kawasaki, *Nature Mater.* 1 (2002) 102..
19. N.G. van der Berg, J.B. Malherbe, A.J. Botha and E. Friedland, *Surf. Interface Anal.* Submitted for publication.
20. W. K Burton, N Cabrera and F C. Frank, *Phil. Trans. Roy. Soc.* 243A (1931) 299.
21. J.P. Hirth and G.M. Pound, *J. Phys. Chem.* 64 (1960) 619.
22. G. Wulff, *Z. Krist.* 34 (1901) 449.
23. T.F. Ciszek, .H. Wang. M.R. Page, R.E. Bauer, and M.D. Landry *IEEE* (2002).
24. T.H. Wang and T.F. Ciszek, *J. Electrochem. Soc.* 147 (2000) 1945.
25. P.D. Ramesh, B. Vaidhyanathan, M. Ganguli and K.J. Rao, *J. Mater. Res.* 9 (1994) 3025.
26. G.D. Papasouliotis and S.V. Sotirchos, *J. Mater. Res.* 14 (1999) 3397.
27. H. Pedersen, S. Leone, A. Henry, V. Darakchieva and E. Janzén, *Surf. Coat. Tech.* 201 (2007) 8931.